Revisiting Diagrams of Ice Growth Environments

Daniel M. Hueholt,[a] Sandra E. Yuter,[a] Matthew A. Miller,[a]

[a] *North Carolina State University, Raleigh, NC*

Daniel M. Hueholt's current affiliation: Department of Atmospheric Sciences, Colorado State University, Fort Collins, CO

Corresponding author: Sandra E. Yuter, seyuter@ncsu.edu

ABSTRACT: Ice habit diagrams published prior to 2009—and many since—do not accurately describe in situ observations of ice shapes as a function of temperature and moisture. Laboratory studies and analysis of field observations by Bailey and Hallett in a series of papers in 2002, 2004, and 2009 corrected several errors from earlier studies, but their work has not been widely disseminated. We present a new, simplified diagram based on Bailey and Hallett's work that focuses on several ice growth forms arising from the underlying surface processes by which mass is added to a crystal: tabular, columnar, branched, side branched, two types of polycrystalline forms, and a multiple growth regime at low ice supersaturations. To aid interpretation for a variety of applications, versions of the ice growth diagram are presented in terms of relative humidity with respect to water as well as the traditional formats of relative humidity with respect to ice and vapor density excess. These diagrams are intended to be understandable and useful in classroom settings at the sophomore undergraduate level and above. The myriad shapes of pristine snow crystals can be described as the result of either a single growth form or a sequence of growth forms. Overlays of data from upper air soundings on the ice growth diagrams aid interpretation of expected physical properties and processes in conditions of ice growth.

CAPSULE: A simplified ice crystal growth form diagram plotted as a function of relative humidity with respect to water and temperature based on previous field and laboratory research.

1. Introduction

Accurate depictions of ice shape as a function of air temperature and moisture are vital throughout meteorology. Globally, clouds containing ice occur with a frequency of approximately 50% (Hong and Liu 2015). Cirrus clouds alone account for nearly 20% of global cloud fraction (Liou 1986; Sassen et al. 2008). Ice crystal shapes, also known as habits, constrain cloud radiative properties and precipitation formation (Wendisch and Yang 2012; Liou and Yang 2016). When snow reaches the surface, ice crystal shapes within snowpacks influence metamorphism (Miller et al. 2017). The expected characteristics of ice growth at given temperatures and relative humidities provide key assumptions for retrieval of ice properties using remote sensing methods (e.g., Yang et al. 2018). Ice crystal shapes are usually visualized using an ice habit diagram, where temperature is placed on one axis, some measure of supersaturation is placed on the other axis, and the habits are denoted on this phase space. However, an internet search for "ice habit diagram" reveals a problem—many of the available figures disagree.

Unfortunately, ice habit diagrams published prior to 2009—and many since—do not accurately describe in situ observations of atmospheric ice. Popular science and internet educational sources intended for classroom use contain errors, such as omitting polycrystals at temperatures less than -20°C, displaying dendrites at low supersaturations near 0°C, or describing ice shapes as periodic with respect to temperature (e.g., Furukawa and Wettlaufer 2007; Libbrecht 2017, 2020; UCAR 2020). While some more recent editions of widely-used textbooks have accurate information (e.g., Wang 2013; Rauber and Nesbitt 2018), others contain outdated materials (e.g., Houze 2014). Errors in upper-level textbooks likely propagate to introductory meteorology texts (e.g., Hakim and Patoux 2017; Ahrens and Henson 2018). This state of confusion makes it difficult to teach accurate information about ice crystal shapes to all levels of students.

The shapes resulting from atmospheric ice growth by vapor deposition as a function of temperature and moisture between 0°C and -70°C are well established. Three papers by Bailey and Hallett (2002, 2004, 2009) based on extensive field observations and laboratory experiments made major changes to previous work and represent the current state of the art. First, at air temperatures below

-20°C, they show ice crystals are predominantly polycrystalline (consisting of multiple elements at different orientations separated by boundary structures). Platelike polycrystals grow between air temperatures -20°C and about -45°C, and columnar polycrystals grow at temperatures less than about -45°C, with a weak dependence on moisture near the interface of the two regions. Second, at low ice supersaturations and most temperatures, vapor deposition yields multiple ice shapes (polycrystals, plates, irregulars, compact crystals, short columns and equiaxed crystals). Bailey and Hallett (2002) describes the platelike polycrystals and explains how prior research was biased by nucleation and substrate effects. Bailey and Hallett (2004) uses a wider range of experimental conditions, and showcases columnar polycrystals and shapes at low ice supersaturations. Bailey and Hallett (2009) presents a new ice habit diagram to combine both their previous laboratory results and extensive field observations across a broad range of environments. The results of Bailey and Hallett (2002, 2004, 2009) have since been supported by subsequent field observations and independent analyses (Gallagher et al. 2005, 2012; Fridlind et al. 2012; Zhu et al. 2015; Fridlind et al. 2016; Lawson et al. 2019; Midzak et al. 2020; Magee et al. 2021). Details of the mesoscopic and crystallographic physics that produce individual ice crystals remain an ongoing area of research (Harrison et al. 2016; Libbrecht 2017; Nelson and Swanson 2019).

The Bailey and Hallett (2009) habit diagrams have not been widely disseminated into textbooks and other educational materials, likely because their figures are complex and intended for an expert audience. We present ice growth diagrams to describe in situ observations of atmospheric ice based on the science of Bailey and Hallett (2002, 2004, 2009) that are intended to be accessible by students and popular science sources while facilitating meteorological data visualization. We do not intend these simplified diagrams to replace specialized materials used for ice microphysics and crystallography research (e.g., Otte and Crocker 1965). We make four key changes designed to lower the cognitive load: swapping the axes, casting the diagram in terms of relative humidity with respect to water (RH_w), focusing on the main direction or pattern of growth rather than ice habit, and restricting the phase space to common tropospheric conditions. This revisualized ice growth diagram is intended for use at sophomore undergraduate level and above. Example classroom activities that utilize the ice growth diagrams were tested in undergraduate and graduate classes and are provided in Appendix A.

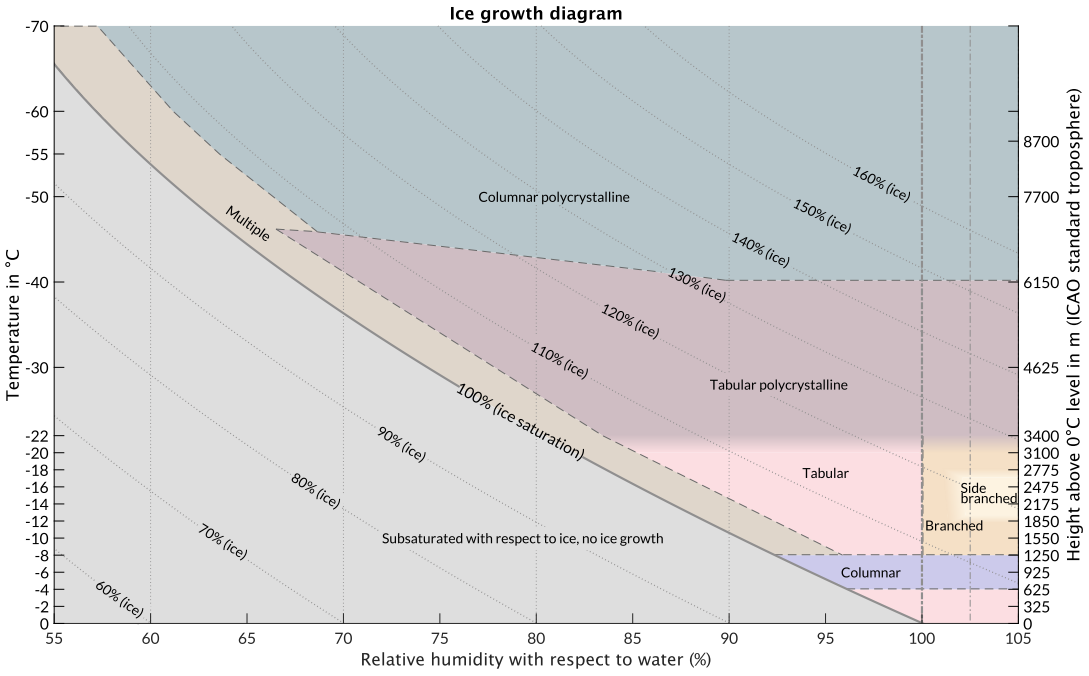

FIG. 1. Ice growth forms diagram in terms of relative humidity with respect to water (RH_w) with contours of relative humidity with respect to ice (RH_{ice}) overlaid. The ICAO approximation on the right y-axis is offset by the height of the 0 °C level. $T_{ice} = T_{air}$ is assumed (St-Pierre and Thériault 2015). Dashed lines indicate uncertainty in the exact bounding conditions between different ice growth forms. Blurred regions indicate transition zones between ice growth forms.

Our ice growth diagram describes ice growth forms resulting from vapor deposition only. Riming adds ice mass through freezing of supercooled cloud droplets on ice crystals and is not included on the diagram. Supercooled droplets can grow and persist when $RH_w \geq 100\%$. Sublimation can also modify ice shapes, in effect eroding them to yield more rounded shapes (Järvinen et al. 2016). Secondary ice production occurs through the shattering of supercooled drops as they freeze which yields tiny ice fragments (Hallett and Mossop 1974; Lauber et al. 2018; Korolev et al. 2020). After secondary ice fragments are produced, they may add mass through vapor deposition. The ice growth form will correspond to the conditions where the particle is located. The typical temperature range for secondary ice production is approximately -3 °C to -10 °C (Hallett and Mossop 1974; Korolev et al. 2020). This overlaps the temperature range of the columnar growth form (-4 °C to -8 °C).

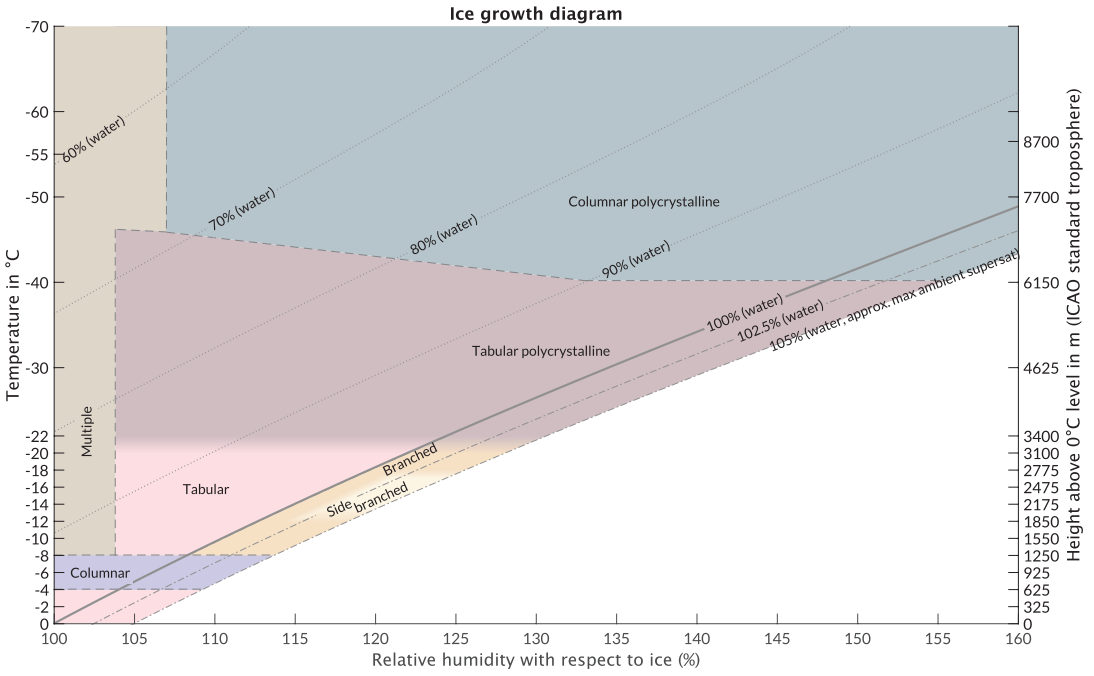

FIG. 2. Ice growth forms diagram in terms of RH_{ice} with contours of RH_w overlaid. The ICAO approximation on the right y-axis is offset by the height of the 0 °C level. $T_{ice} = T_{air}$ is assumed (St-Pierre and Thériault 2015). Dashed lines indicate uncertainty in the exact bounding conditions between different ice growth forms. Blurred regions indicate transition zones between ice growth forms.

2. Revisualized ice growth diagram

We introduce a version of the ice growth diagram using relative humidity with respect to water (RH_w) (Fig. 1) in addition to the traditional displays of relative humidity with respect to ice (RH_{ice}) (Fig. 2) and vapor density excess (Fig. 3). Appendix B has alternate versions of these diagrams with higher-contrast colors designed for use as base layers in data visualization as well as information on the publicly available software to plot and customize the diagrams. The exact temperature and moisture conditions separating different ice growth forms are not known precisely and we use dashed lines to indicate this uncertainty in the diagram. The well-documented transition zones between tabular monocrystal and tabular polycrystalline forms and between branched and side branched forms (Nakaya 1954; Bailey and Hallett 2009; Takahashi 2014) are blurred in the

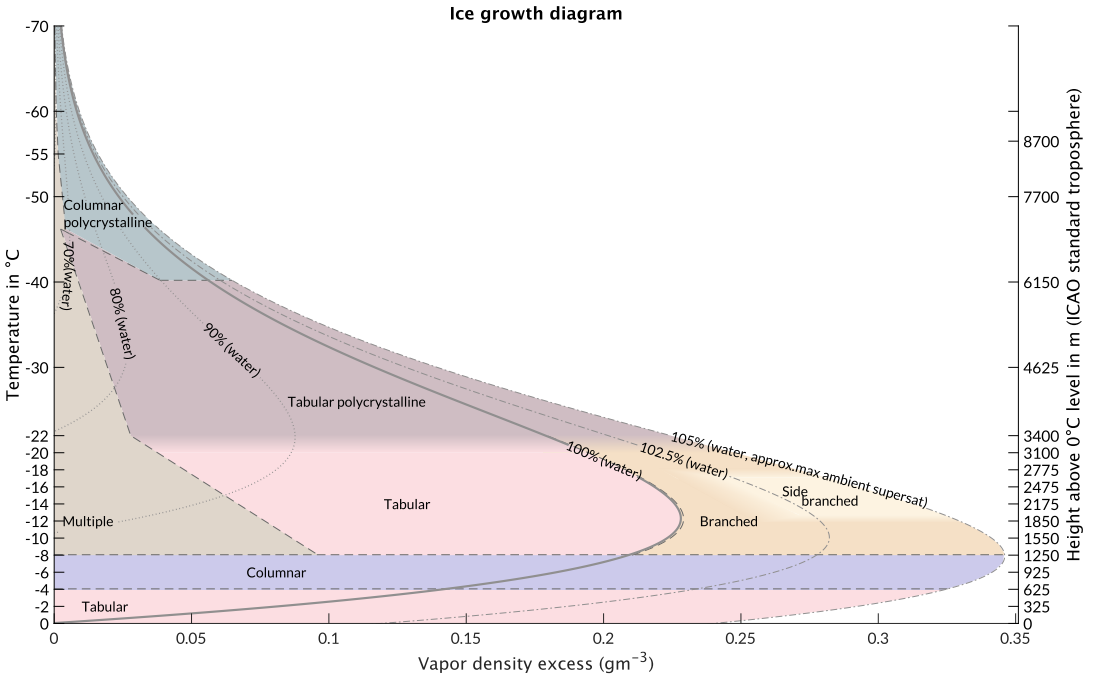

FIG. 3. Ice growth forms diagram in terms of vapor density excess over ice saturation with contours of RH_w overlaid. The ICAO approximation on the right y-axis is offset by the height of the 0 °C level. $T_{ice} = T_{air}$ is assumed (St-Pierre and Thériault 2015). Dashed lines indicate uncertainty in the exact bounding conditions between different ice growth forms. Blurred regions indicate transition zones between ice growth forms.

diagram. In all diagrams, the temperature of the ice and the temperature of the air are assumed to be equal, i.e. $T_{ice} = T_{air}$ (St-Pierre and Thériault 2015).

a. Simplify to ice growth form rather than ice habit

One reason for the complexity of Bailey and Hallett's diagram is its focus on ice habit. Systematic habit classifications have grown unwieldy, as the number of identifiable habits increased from the 42 in Nakaya (1954) to the 121 identified by the current standard (Kikuchi et al. 2013). Researchers continue to identify novel crystal habits (Vázquez-Martín et al. 2020). No mapping exists to relate all these unique ice shapes to the environmental conditions in which they form. Further obfuscating the situation, the names of ice shapes are used inconsistently (Bailey and Hallett 2002, 2004).

Our diagrams describe the main growth direction or growth pattern of a crystal, which we call the ice growth form. While there are a huge number of habits, there are only a few basic

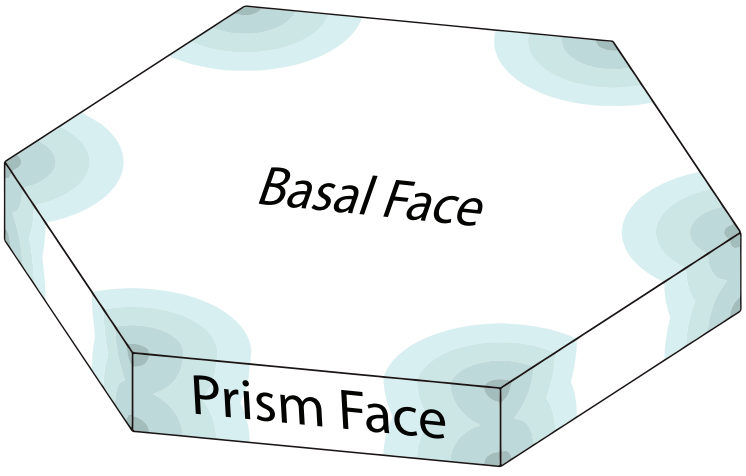

FIG. 4. Basal and prism faces on an idealized hexagonal plate crystal resulting from the tabular growth form. Shading indicates relative step growth rates with darker shading indicating faster growth. Adapted from Frank (1982).

growth forms: tabular, columnar, branched, and side branched. Tabular or columnar growth forms occur as polycrystals when discontinuities separate regions of a particle with distinct crystalline orientations. The ice growth forms arise from the underlying crystal surface processes by which ice mass is added to the crystal. When a crystal is located in an environment with RH_{ice} greater than 100%, it can gain mass through vapor deposition. This mass attaches to the crystal in steps centered on the corners, where the vapor density excess is highest (Frank 1952; Hobbs and Scott 1965; Frank 1982). New crystal growth will then spread as layers along the basal face, prism face, or protrude outward from the corners (Fig. 4) depending on local thermodynamic conditions (Burton et al. 1951; Hallett 1961; Mason et al. 1963; Nelson and Knight 1998; Sazaki et al. 2010). Temperature determines the overall tabular or columnar form by controlling whether the prism or basal face experiences the fastest growth rate (Mason et al. 1963; Nelson and Knight 1998). In the presence of a large supersaturation, new steps will be added more quickly than the growth layer can spread across a face, producing a main growth direction outward from the corner (Frank 1982; Libbrecht 2005). In a polycrystalline growth form, multiple regions of different crystalline orientation separated by discontinuities such as grain boundaries grow simultaneously (Kobayashi et al. 1976; Furukawa and Kobayashi 1978; Iwai 1986; Bailey and Hallett 2002, 2004). The individual elements of the polycrystal grow on either their prism or basal face, producing distinct tabular or columnar polycrystalline forms.

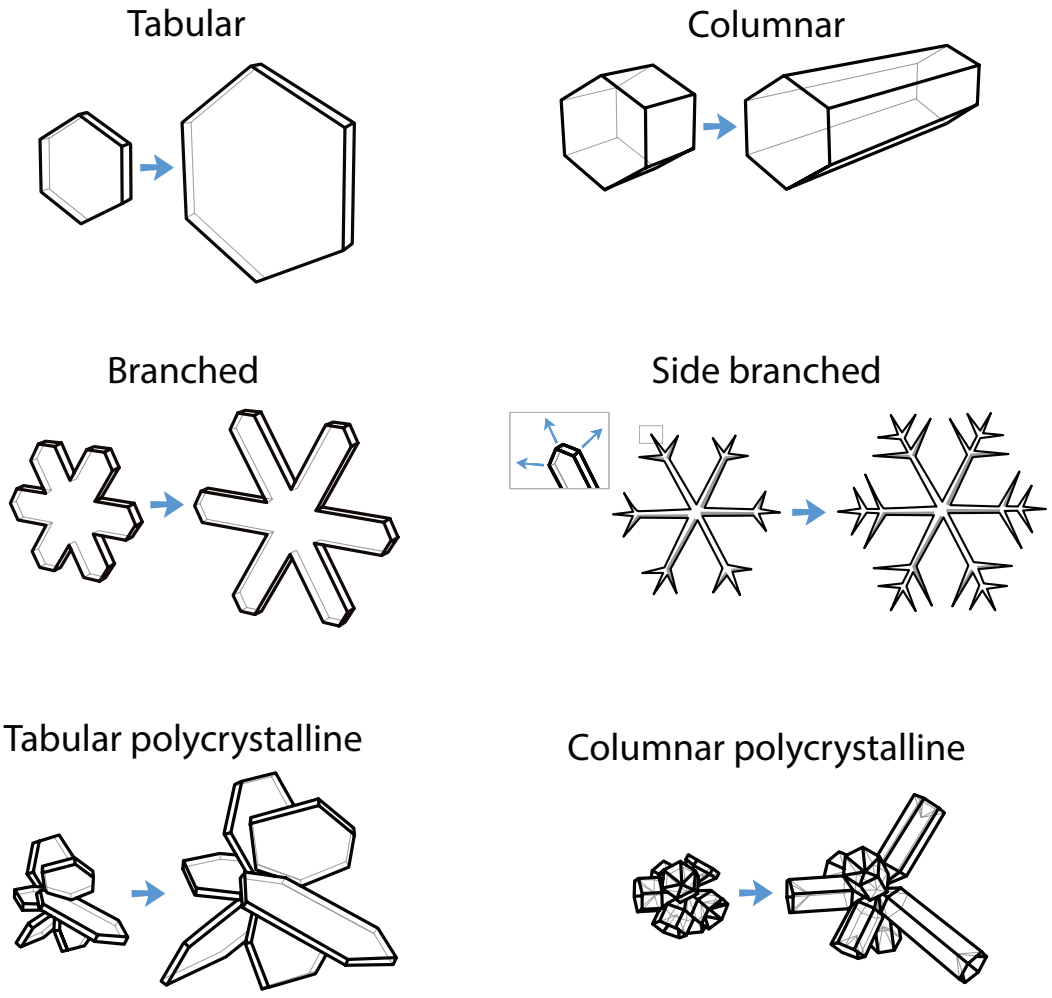

120 FIG. 5. Illustrations of the main ice growth forms in the troposphere. Each pair shows a sequence of a single
121 growth form with a particular archetypal shape. See text in Section 2a for further details.

148 Figure 5 shows schematics of archetypal crystals undergoing the different growth forms. The
149 nomenclature uses naming conventions that are more understandable to the non-specialist than
150 either the Miller-Bravais index or crystallographic axis systems (e.g., Otte and Crocker 1965;
151 Libbrecht 2005; Hoffmann 2020).

152 **Tabular:** Yields a plate-like monocrystal with much more width than depth. Main growth
153 direction is out from the prism face. The layer growth rate along the prism faces and the step
154 growth rate at the corners are in balance.

155 **Columnar:** Produces an elongated monocrystal with much more depth than width. Main growth
156 direction is out from the basal face. The layer growth rate along the basal faces and the step growth

rate at the corners are in balance.

Branched: Produces a sectored plate-like monocrystal with much more width than depth. The main growth direction is out from the corner. The initial branching occurs when step growth rates at the corners greatly exceed the layer growth rate along the prism face such that the corner grows out from the prism face.

Side branched: Results in a fernlike, dendritic monocrystal. This is a special case of branched growth where the step growth rates are so high that there is repeated branching.

Tabular polycrystalline: Produces crystals consisting of multiple plate-like elements at different orientations. Simultaneous tabular growth occurs along multiple axes with crystal discontinuities separating regions of different crystalline orientation formed by a polycrystalline ice nucleation event. Examples include crossed plates, spearheads, and assemblages.

Columnar polycrystalline: Produces crystals consisting of multiple columnar-like elements at different orientations. Simultaneous columnar growth occurs along multiple axes, with crystal discontinuities separating regions of different crystalline orientation formed by a polycrystalline ice nucleation event. Examples include bullet rosettes, column rosettes, and basals with columns.

Multiple: At low supersaturations with respect to ice, multiple growth forms–tabular, columnar, tabular polycrystalline, and columnar polycrystalline–can co-occur. Can yield compact crystals including equiaxed crystals, short columns, and irregulars when growth rates after ice nucleation are extremely low.

Our use of the term “tabular” and “columnar” is consistent with Nelson and Knight (1998), who use these terms for crystals with aspect ratios less than 1 or greater than 1, respectively. “Branched” is used in Libbrecht (2005) to describe growth producing sectored crystals. Nelson (2005) and Libbrecht (2017) use “side branched” to specify fernlike crystals. “Tabular polycrystalline” is intended to be synonymous to the “platelike polycrystals” discussed in Bailey and Hallett (2002, 2004, 2009). “Columnar polycrystalline” is used by Bailey and Hallett (2004, 2009). “Tabular polycrystalline” and “columnar polycrystalline” are used for consistency with “tabular” and “columnar” monocrystal forms. We use the label "polycrystalline growth form" for ice crystals that are nucleated as polycrystals while they remain in the environment where polycrystal nucleation occurs. This terminology is consistent with Bailey and Hallett (2004, 2009, 2012)

The growth of polycrystalline forms is distinct from aggregation. Polycrystalline forms involve tabular or columnar growth occurring simultaneously on elements separated by discontinuities, such as grain boundaries. The elements' crystal lattices are intertwined and grow together from the initial nucleation event. Aggregation involves multiple crystals that grow separately, then later happen to collide and jumble together. Aggregation rearranges preexisting ice mass per unit volume with no significant thermodynamic impact. An aggregate may experience further growth through vapor deposition after formation.

These ice growth forms describe the typical ice crystals encountered in the clouds and precipitation of Earth's atmosphere, but are not intended to be fully comprehensive. Bundles are characterized by multiple columnar crystals (e.g., needles, columns, sheaths) growing in parallel from a common center (Nakaya 1954; Magono and Lee 1966; Frank 1982; Kikuchi et al. 2013; Nelson and Swanson 2019). Bundles occur in the same temperature range as the columnar growth form, but their required supersaturation has not been quantified (Takahashi et al. 1991; Nelson and Swanson 2019). Thus, we are unable to place bundles on our diagrams. While our classification system includes the typical ice known today, future observations may identify new ice growth forms. Finally, unique ice growth processes can occur at extreme conditions, such as near 200% RH_w or in strong electric fields (Hallett and Mason 1958; Crowther and Saunders 1973; Libbrecht 2003). Such conditions are not in the domain of our diagrams.

The same ice growth form can yield ice shapes with different properties. For example, while both hollow and solid bullet rosettes are formed through columnar polycrystalline growth, each has a distinct scattering phase function (Yang et al. 2008; Järvinen et al. 2018). This illustrates the different affordances of systematic classifications, as compared to ice growth forms. Systematic classifications give detail about individual ice shapes but little information about how they form. Our growth forms efficiently describe how ice grows, but need to be supplemented when properties of specific shapes are important.

When an ice crystal encounters multiple environments corresponding to different ice growth forms, a sequence of different types of growth occurs (Nakaya 1954; Hallett and Mason 1958; Bailey and Hallett 2004, 2009). Examples of sequential growth are discussed in Section 5.

Other authors have portrayed ice growth as a function of thermodynamics in terms of the primary axis of growth (Wood et al. 2001). The presentation of those diagrams has been tailored towards

experts, and some are based on models with invalid assumptions derived from laboratory work (Bailey and Hallett 2002, 2004, 2009).

b. Display decreasing temperature on the y-axis

Almost all published ice habit diagrams place temperature on the x-axis and the unit of moisture (traditionally supersaturation with respect to ice or vapor density excess) on the y-axis. The earliest research into ice habit considered only the effects of temperature (Heim 1914; Weickmann 1945; aufm Kampe et al. 1951; Mason 1953). The first plots of ice shape simply displayed a temperature axis and indicated shapes as appropriate. When moisture began to be considered, temperature remained on the abscissa and supersaturation began to be used as the ordinate (Nakaya and Sekido 1936; aufm Kampe et al. 1951; Nakaya 1954).

Swapping the axes to place decreasing temperature on the y-axis and moisture on the x-axis yields several interpretive advantages (e.g., Fig. 1). Having temperature decrease on the y-axis mirrors the real atmosphere, where temperature generally decreases with height. This removes a layer of abstraction, simplifying interpretation in terms of the physical atmosphere. The International Civil Aviation Organization (ICAO) standard reference atmosphere maps temperature to height (ICAO 1993). The scale is offset by the height of its 0°C level on the right side of the diagram. This height scale is intended to encourage intuition for students about where these temperatures qualitatively occur in the mid-latitude troposphere. Individual observed atmospheric profiles are often very different from this reference atmosphere. Deviations can be large in convection, near air mass boundaries, or in the tropics. Bailey and Hallett presented a version of their diagram with temperature on the y-axis and an atmospheric height approximation in a 2010 conference paper (Bailey and Hallett 2010).

c. Use RH_w

We favor the version of the diagram using RH_w on the x-axis with RH_{ice} contours overlaid (Fig. 1) especially for undergraduate-level educational materials. RH_w is used throughout meteorology, while ice supersaturation and vapor density excess are more specialized. RH_w is also widely understood, at least intuitively, by the general public due to its use in weather forecasts. To the best of our knowledge, our diagram in Figure 1 is the first to illustrate ice growth in terms of RH_w.

In the appendix, Figure B1 shows the RH_w version simplified to emphasize only the subsaturated and supersaturated conditions that occur in different portions of the diagram. We provide this figure as an educational tool to scaffold basic concepts of ice microphysics in introductory classes, before introducing the diagram with ice growth forms. The presentation highlights the relationship between RH_w and RH_{ice} as a function of temperature. As air temperature decreases, the RH_w needed to sustain an ice cloud shrinks as well. This is in contrast to the requirement that $RH_w \geq 100\%$ for liquid phase and mixed phase clouds.

Ice supersaturation directly relates to ice growth through deposition, which can only occur above saturation with respect to ice, and ice loss through sublimation, which occurs when conditions are subsaturated with respect to ice. Diagrams in terms of ice supersaturation include Nakaya (1954), Kobayashi (1957), Hallett and Mason (1958), Bailey and Hallett (2009), and St-Pierre and Thériault (2015). Vapor density excess describes the density of water vapor in excess of saturation with respect to ice (units g m^{-3}). Diagrams in this format include Kobayashi (1961), Pruppacher and Klett (1997), Furukawa and Wettlaufer (2007), St-Pierre and Thériault (2015), and Libbrecht (2017). Vapor density excess is a concrete way to describe the physical quantity of water vapor, rather than expressing some percentage of saturation.

d. Restrict phase space to conditions common in the troposphere

Our diagrams extend to -70°C, as in Bailey and Hallett (2009). These temperatures are colder than typical values in the mid-latitude troposphere to better encompass convective anvils and temperatures near the tropical tropopause (Lawson et al. 2006; Midzak et al. 2020). Field observations of atmospheric ice at temperatures less than -70°C are sparse, but indicate there are no further changes to the ice growth form to at least -90°C (Woods et al. 2018). By convention, the top of the mid-latitude troposphere is considered to be -56.5°C (ICAO 1993). For applications in the mid-latitudes, this temperature constraint may be more appropriate. The code given in Appendix B allows for the boundaries of any of our diagrams to be modified at the user's discretion.

We bound all of our diagrams at a maximum *ambient* RH_w of 105% based on theoretical and observational arguments from Korolev and Mazin (2003). Ambient supersaturations with respect to water (RH_w>100%) can occur within updrafts when the rate of change of the equilibrium saturation vapor pressure with decreasing temperature (source) is faster than the condensation

rate on activated cloud condensation nuclei and existing drops (sink) (Rogers and Yau 1989). Supersaturations with respect to water > 1% are rare and ephemeral (Mason 1971; Gerber 1991). Aircraft and radiosonde in situ measurements of temperature and moisture characterize ambient RH. There are no changes to the growth form for naturally occurring values of RH_w> 105% for any temperature.

Ventilation is an important factor in ice crystal growth by vapor deposition and occurs for falling ice particles when there is nonzero airflow around a crystal, as occurs when a crystal is falling and/or advected by horizontal wind, updrafts or downdrafts (Hallett and Mason 1958; Keller and Hallett 1982; Takahashi et al. 1991; Fukuta and Takahashi 1999). Ventilation acts to enhance the vapor density immediately adjacent to a crystal's outer edges, thus increasing the local RH at the crystal over the ambient value (Pruppacher and Klett 1997; Keller and Hallett 1982; Wang 2002; Bailey and Hallett 2004). Quantifying the enhancement of supersaturation due to ventilation requires knowledge of particle size, shape, and fall speed (Heymsfield 1975; Hall and Pruppacher 1976; Johnson 1997; Ji and Wang 1999). Due to computational complexity, modeling studies of even simplified shapes (such as spheres or columns) have largely been restricted to qualitative descriptions of the vapor field (Wang 2002; Bailey and Hallett 2004). Ventilation effects can yield locally higher RH at the corners as compared to the straight edges of the same crystal (Wang 2002). For a given temperature, one can infer ice ventilation effects by shifting ambient RH values to the right on the diagram (see Section 5).

We do not use the RH limit from Bailey and Hallett (2009) which is based on the estimated maximum supersaturation with ventilation and is approximated by twice the ice supersaturation at RH_w = 100% for each temperature (which is distinct from both RH_w = 200% and RH_{ice} = 200%). This value is intended to represent the upper bound on the local conditions experienced *at* a growing crystal (Bailey and Hallett 2004). However, this method limits the ventilation ice supersaturation close to RH_w = 100% at temperatures near 0 °C, where conditions consistent with larger ambient supersaturations are observed to occur (Korolev and Mazin 2003; Cronce et al. 2007; Ganetis et al. 2018). At low temperatures, such as near -65 °C, the estimated maximum supersaturation with ventilation method from Bailey and Hallett (2009) yields maximum RH_{ice} of 262% (RH_w = 145%). In convective clouds with strong vertical motions, observations show ambient moisture values at these temperatures are never in excess of RH_{ice} = 160% (RH_w = 88.3%)

(D'Alessandro et al. 2017). Even with ventilation, the equivalent of RH_w = 145% at -65 °C seems implausibly high. At the user's discretion, the code provided in Appendix B includes an option to plot the Bailey and Hallett (2009) estimate of maximum supersaturation with ventilation on the diagram.

Laboratory work has demonstrated unique ice growth behavior at extreme supersaturations in certain temperature ranges. High-temperature (0°C to -4°C) dendrites require RH_w values of up to 200% (Hallett and Mason 1958). Since these supersaturations are far beyond what could be achieved in either the ambient or with ventilation, they cannot occur in Earth's atmosphere (Korolev and Mazin 2003; Bailey and Hallett 2004) and we exclude these from our diagrams.

3. Ice growth forms from atmospheric profiles

Profiles of temperature and RH_w from observations or models can be plotted on the diagram to reveal the ice growth forms. In this manner, soundings datasets can be used to describe the distribution of ice growth forms. This is a novel use of soundings data. Overlaying weather and climate numerical model output on the diagram allows one to interpret the model's implied ice growth forms, and to evaluate how predicted growth forms compare to observations.

When interpreting observed radiosonde data overlaid on the ice growth diagram, several caveats need to be kept in mind. Commercial radiosondes cannot measure ambient supersaturations with respect to water. In particular, this means these data cannot be used to identify precisely where side branched growth occurs. Qualitatively, we infer higher probabilities for branched and side branched growth by ventilation for the subset of points with RH_w > 95% in the proper temperature range. The radiosonde characterizes the environment, not any individual crystal. Precipitation-sized ice experiences a sequence of growth conditions as it falls (sediments) and will also experience ventilation.

We contrast winter season radiosonde data sets from December 2014 through February 2015 from a midlatitude maritime, a polar, and a midlatitude continental site in the Northern Hemisphere in Figure 6. All soundings during the period are used in these plots whether clouds and precipitation were present or not. These three examples illustrate the prevalence of conditions for the polycrystalline and multiple growth forms within the colder cloud tops at all three locations.

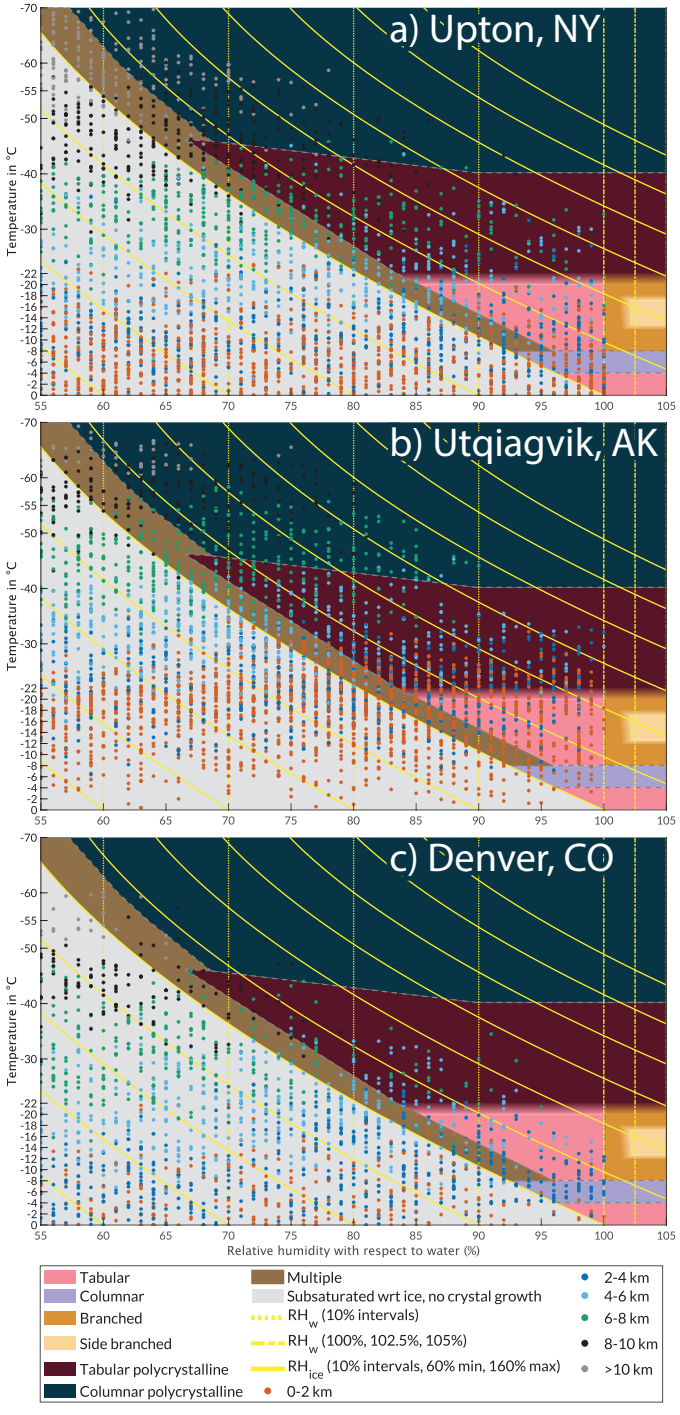

FIG. 6. Seasonal radiosonde data for three locations during the winter of December 2014 through February 2015 overlaid on the ice growth form diagram. Data points are plotted with air temperature as the vertical coordinate. a) From the NWS radiosonde site at Upton, NY (178 profiles). b) From the DOE radiosonde site at Utqiagvik, AK (180 profiles). c) From the NWS radiosonde site at Denver, CO (179 profiles). Dot colors represent altitude of measurements in 2-km intervals. See key for details.

The example midlatitude maritime environment is from the National Weather Service's (NWS) sounding site in Upton, NY (Fig. 6a). The most frequent ice growth conditions involve relatively warm temperatures—the points are clustered most densely between 0°C and -10°C. In comparison, there are few points near water saturation in the -12°C to -18°C range.

We use the Department of Energy (DOE) Atmospheric Radiation Measurement North Slope Alaska Central Facility research site in Utqiagvik, AK above the Arctic Circle and along the coast of the Beaufort Sea as our polar environment example in Figure 6b (DOE-ARM 2020). As expected, these profiles are colder than in the midlatitudes. Ambient conditions favor tabular, tabular polycrystalline, and columnar polycrystalline growth, along with the multiple regime.

The example midlatitude continental location is the National Weather Service's radiosonde site in Denver, CO (Figure 6c). As an interior continental site, Denver's seasonal profile is far drier than either Upton, NY or Utqiagvik, AK. There are very few points near water saturation in the -12°C to -18°C range. The overall sparseness of points within the ice growth regions of the diagram indicates background ambient conditions at Denver were rarely sufficient to maintain ice growth. In addition to synoptic-scale vertical motions along air mass boundaries, mesoscale upslope flows and vertical motions from waves such as those forced by topography are likely critical to locally enhance supersaturations within clouds in this region.

4. Rapid ice growth conditions encompass more than dendrites

The higher the vapor density excess over ice saturation, the faster the vapor deposition growth rate for a given moisture content of the air (water vapor mixing ratio) will be (Rogers and Yau 1989; Houze 2014; Harrison et al. 2016). The air temperature corresponding to the peak vapor density excess varies with RH_w (Fig. 3). When accounting for the influence of latent heat released from deposition, peak growth rates occur near -15°C for environments near saturation with respect to water (Ryan et al. 1976; St-Pierre and Thériault 2015). High vapor density excess above 0.25 g m^{-3} can occur for temperatures between just below 0°C to -19°C and encompasses the tabular, columnar, branched, and side-branched growth forms but not the polycrystalline or multiple growth forms. Growth rate also depends in part on the starting size of the crystal (Harrison et al. 2016).

The temperature range -12°C to -18°C is sometimes labeled the "dendritic growth zone" and is often emphasized as a region of rapid ice growth (Kumjian et al. 2014; Rauber et al. 2017; Demange

et al. 2017; NWS 2017). Since the formation of dendrites requires both temperatures between -12°C to -18°C and $RH_w \gtrapprox 101.5\%$, it is mistaken to infer the production of these crystals based only on temperature conditions. Ventilation can nudge crystals growing at lower supersaturations in this temperature range into the side branched growth region, producing dendrites. The enhancement from ventilation is difficult to quantify and may not necessarily be sufficient to reach conditions with $RH_w \gtrapprox 101.5\%$. Nelson (2005) suggests that side branching is related to growth rate fluctuations. Referring to the -12°C to -18°C temperature range as a dendritic growth zone implies the production of a specific habit that will not always occur. Further, dendrites are an unrepresentative subset of the possible varieties of crystals produced by the side branched growth form (Korolev et al. 1999; Bailey and Hallett 2009; Libbrecht 2017). Fundamentally, there is no set of atmospheric conditions that guarantees dendrites will occur exclusively. We suggest retiring the term "dendritic growth zone" for the -12°C to -18°C temperature range. Misinterpretation and overemphasis of the "dendritic growth zone" is in part responsible for the mistaken impressions among students that other ice growth forms cannot gain mass rapidly and that snow primarily consists of dendrites.

5. Sequential growth

An ice crystal can grow as a sequence of distinct ice growth forms as it falls through different temperature and moisture conditions. The resulting ice crystal shape can be described by this sequence of growth forms. Growth sequences can be identified using data from high-resolution particle imagers such as the SPEC Inc. Cloud Particle Imager (CPI), Particle Flux Analytics Multi-Angle Snowflake Camera, and the Karlsruhe Institute of Technology Particle Habit Imaging and Scattering Probe (PHIPS) (Lawson et al. 2001; Garrett et al. 2012; Abdelmonem et al. 2016). These sequences can reveal the history of the thermodynamic conditions that the crystal encountered. One of the earliest researchers to study atmospheric ice, Ukichiro Nakaya, notably phrased this as “A snow crystal is a letter from the sky” in his seminal 1954 work (Nakaya 1954). Bailey and Hallett (2009) describe mixed-habit rosettes in terms of sequential growth, specifically, columnar polycrystalline followed by tabular polycrystalline growth. In Figure 7, we show examples of two other shapes that can be described by their growth form sequences. The images are from the PHIPS mounted on the NASA P-3 aircraft during the Investigation of Microphysics and Precipitation for Atlantic Coast-Threatening Snowstorms (IMPACTS) field campaign in 2020 (McMurdie et al.

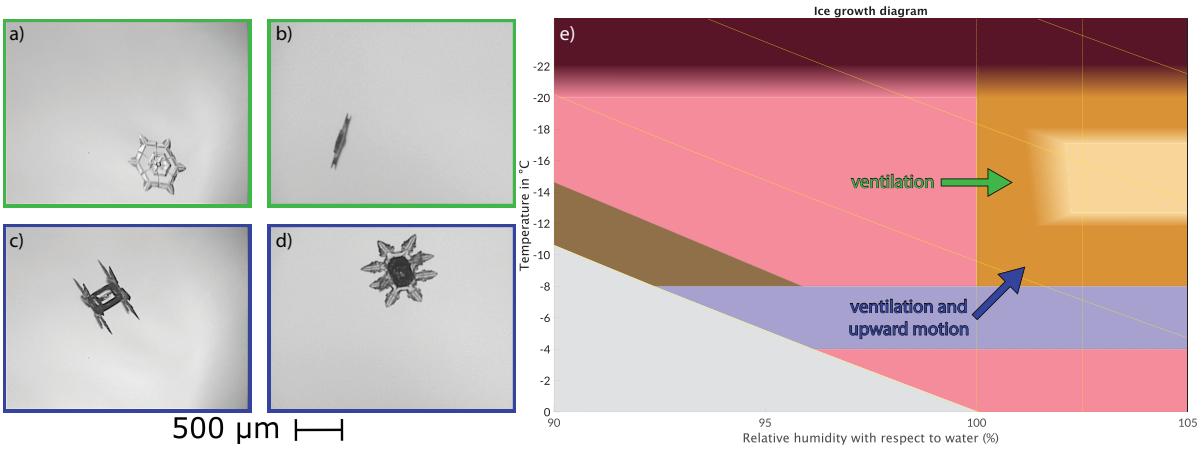

FIG. 7. Examples of sequential growth with possible physical pathways annotated on g) the ice growth form diagram. Colors of annotations on f) correspond to colors bordering the PHIPS image pairs. Image pairs are different views of the same particle; all are from the 25 Jan 2020 IMPACTS flight. a) and b) Images obtained at 22:57 UTC at 4.8 km altitude of a crystal formed by a sequence of tabular growth followed by branched growth. Kikuchi et al. (2013) classification: plate with branches, P4e. c) and d) Images obtained at 22:25 UTC at 4.9 km altitude of a crystal formed by a sequence of columnar growth followed by branched and then side branched growth. Kikuchi et al. (2013) classification: column with dendrites, CP1b.

2022, 2019; NASA 2020). These ice particles were likely observed at lower altitudes and in different conditions than where the ice crystals initially formed and grew.

An example of a "plate with branches" or "P4e" habit is shown in Figure 7ab. We identify the sequence yielding this crystal as tabular growth (forming the central hexagonal plate) followed by branched growth (yielding the 6 sector branches). An enhancement of the local supersaturation by ventilation is likely responsible for this sequence. Tabular growth requires only suitable temperatures and a small supersaturation with respect to ice. Ventilation can then increase the supersaturation local to the crystal such that branched growth begins. Qualitatively, reviewing large numbers of CPI and PHIPS images indicates many branched and side branched crystals, including dendrites, have an inner core of a hexagonal plate. This implies branched crystals are commonly produced by sequences of tabular and branched growth, as has been suggested by prior laboratory work (Fukuta and Takahashi 1999). The in situ environmental conditions when the images were obtained were RH_{ice} = 113.5%, RH_w = 98.4%, and T_{air} = -14.3°C. While these ambient conditions

correspond to tabular growth, ongoing ventilation may support branched growth by enhancing the supersaturation local to the crystal.

An example of the habit informally known as "capped column" (Libbrecht 2017) is shown in Figure 7cd. Kikuchi et al. (2013) classifies this as "column with dendrites" or "CP1b" (their Fig. 1-CP1b). The sequence producing this crystal is columnar growth (forming the central column) followed by branched growth (producing the sectored platelike caps on the ends) and then side branched growth (yielding the further branches off the initial six branches). The small side branches are best seen in Fig. 7f. Upward motion, accompanied by ventilation, is a possible physical pathway for this sequence. The crystal must both be cooled below -8°C and moistened above water saturation to switch from columnar growth to branched growth. An enhancement of supersaturation alone, as caused by ventilation, cannot yield this sequence. In situ environmental conditions corresponding to the image are RH_{ice} = 99.1%, RH_w = 87.1%, and T_{air} = -13.0°C.

6. Summary and concluding remarks

We revisualize the current state-of-the-art ice habit diagram in Bailey and Hallett (2009) by simplifying the dozens of ice habits to a small number of ice growth forms and recasting the diagram in terms of RH_w with the goals of improving clarity and ease of use for non-specialists. Use of RH_w puts ice microphysics into a more accessible framework for students than RH_{ice} or vapor density excess. The decreasing RH_w needed for ice saturation and cloud formation as a function of decreasing air temperature is readily apparent. The important distinction that branched growth requires supersaturation with respect to water whereas all other growth forms do not is shown clearly.

In addition to the educational applications (Appendix A), we see several pathways to apply the ice growth diagram in research. We think it is possible that many, if not all, observed pristine ice shapes are reducible to their component growth form sequences. Joint analysis of high-resolution ice particle images and thermodynamic profiles in the context of the ice growth diagram has the potential to yield a classification system for ice crystals based on their sequence of growth forms. Plotting atmospheric profiles from observed radiosonde data and weather and climate model output on the ice growth diagram can provide insight on where and why differences between model physics and the real atmosphere occur. Analysis of the decades-long radiosonde archive in the context

of the ice growth diagram may yield insights into impacts of the changing climate on ice cloud properties.

Acknowledgments. The development and refinement of the ice growth diagrams benefited from discussions with David Kingsmill. Extensive comments from the anonymous reviewers as well as suggestions from journal editors Jeff Waldstreicher and Manfred Wendisch were instrumental in improving the clarity and content of the article. Martin Schnaiter provided the NASA IMPACTS PHIPS data (Schnaiter 2020), and Ryan Bennett supplied the NASA P-3 flight-level data (Yang Martin 2020). Aaron Bansemer and David Delene provided early access to the NASA IMPACTS particle image datasets. Special thanks to Laura Tomkins, Levi Lovell, and Ronak Patel for their input on visualization options, and to Luke Allen for NASA P-3 data processing. Figure 5 artwork by Lenni Armstrong. Christina Cartwright edited the manuscript. This work was supported by the National Science Foundation (AGS-1347491 and AGS-1905736), the National Aeronautics and Space Administration (80NSSC19K0354), and the North Carolina State University Honors Program (Hueholt). The IMPACTS project was funded by the NASA Earth Venture Suborbital-3 (EVS-3) program managed by the Earth System Science Pathfinder Program Office.

Data availability statement. National Weather Service radiosonde data from Upton, NY and Denver, CO can be obtained from the Integrated Global Radiosonde Archive, Version 2 described in Durre et al. (2006).

Department of Energy Atmospheric Radiation Measurement radiosonde data from the North Slope Alaska Central Facility site at Utqiagvik, AK are accessible from doi.org/10.5439/1021460.

The Investigation of Microphysics and Precipitation for Atlantic Coast-Threatening Snowstorms (IMPACTS) campaign data sets are stored at the NASA Earth Data Archive (https://ghrc.nsstc.nasa.gov/home/). Specific data sets used in this paper are accessible at dx.doi.org/10.5067/IMPACTS/P3/DATA101 for the NASA P-3 Meteorological and Navigation Data and dx.doi.org/10.5067/IMPACTS/PHIPS/DATA101 for the cloud particle imagery collected by the Particle Habit Imaging and Polar Scattering (PHIPS) probe onboard the NASA P-3 aircraft.

PNG, EPS and SVG files for the ice growth diagram variations as well as the MATLAB code and documentation can be accessed at https://osf.io/g9vzj/

APPENDIX A

Example Classroom Exercises

As part of in-class exercises or homework, having students use a diagram that simultaneously illustrates the contexts of air temperature, RH_{ice}, and RH_w can aid understanding of cloud microphysics processes. Two example exercises that use the version of the ice growth diagram with respect to RH_w are presented below. These activities have been tested and refined for use as think-pair-share formative assessments in several undergraduate and graduate courses taught by Yuter. In these standalone exercises, the term RH_{water} is used rather than RH_w.

a. Exercise 1

This activity is used to review concepts on environments associated with different water phase changes. Introductory students can answer the questions by referring to the simplified ice growth diagram (Figure B1). For more advanced students, these questions can serve as a warm-up exercise. *Question*: For each of the following four descriptions of phase changes indicate the corresponding RH_{ice} and RH_{water} values OR indicate that the described set of phase changes for the given temperature range are not physically possible in the real atmosphere. Assume -40 °C < Air Temperature < 0 °C.

1. Sublimation of ice AND evaporation of water droplets
   RH_{water} <100% or RH_{water} >100%
   RH_{ice} <100% or RH_{ice} >100%
   Not physically possible in the real atmosphere

2. Sublimation of ice AND condensation of water droplets
   RH_{water} <100% or RH_{water} >100%
   RH_{ice} <100% or RH_{ice} >100%
   Not physically possible in the real atmosphere

3. Growth of ice by vapor deposition AND evaporation of water droplets
   RH_{water} <100% or RH_{water} >100%
   RH_{ice} <100% or RH_{ice} >100%
   Not physically possible in the real atmosphere

4. Growth of ice by vapor deposition AND condensation of water droplets
   RH_{water} <100% or RH_{water} >100%

RH_{ice} <100% or RH_{ice} >100%

Not physically possible in the real atmosphere

Answers: 1) RH_{ice} < 100% and RH_{water} < 100%; 2) Not physically possible. RH_{ice} is always less than RH_{water} for air temperatures < 0 °C; 3) RH_{ice} > 100% and RH_{water} < 100%; 4) RH_{ice} > 100% and RH_{water} > 100%. Many students, even advanced students, get 2) wrong. Getting an incorrect answer provides an opportunity for the students to learn from their mistake and gain better understanding of the relationship between RH_{ice} and RH_{water} rather than thinking of these quantities as separate.

b. Exercise 2

This exercise asks students to apply concepts using the ice growth diagram and is designed for upper-level undergraduates or first-year graduate students.

Question: Use the ice growth diagram and physical reasoning to answer the following questions:

1. An aircraft probe samples a tabular polycrystal at -20 °C. How could this crystal have formed?

2. An unrimed ice crystal consisting of a column capped with two edge plates is observed at -5 °C and RH_{water} = 90%. Could the edge plates continue to grow in this environment?

3. Branched crystals are observed in an air temperature of -6 °C and RH_{water} = 90%. A vertically pointing radar indicates vertical air motions in the cloud are all $\leq$ 0 m s^{-1} for the last 40 minutes. How could these crystals form?

Answers: 1) The crystal could have formed within the tabular polycrystal region and reached this location by sedimentation. It may also have grown in the mixed growth region—either at -20 °C and RH_{ice} between 100% and 103.8%, or by sedimenting here from other lower temperature mixed growth conditions. 2) No. At this temperature and RH_{water}, the corresponding RH_{ice} is < 100%. 3) Since there is no indication of upward motions, ambient RH_{water} > 100% is unlikely. The condition of $RH_{water} \gtrapprox$ 101.5% necessary for branched growth is likely a result of ventilation increasing vapor pressure immediately adjacent to the falling ice crystal when the crystal was at air temperatures between -12 °C and -18 °C.

528 APPENDIX B

529 **Software for Plotting Ice Growth Diagrams**

530 Our software to plot the ice growth diagrams in formats with muted colors and labels on the
531 diagram (Figs. 1, 2, 3) and with brighter colors and a key at the bottom of the diagram (Appendix
532 Figures B2, B3, B4) is on the Open Science Foundation website. The MATLAB code and
533 documentation can be accessed at https://osf.io/g9vzj/.

534 MATLAB code to plot data from the Integrated Global Radiosonde Archive on the ice growth
535 diagrams is included in the package. The RH_w and RH_{ice} versions are better suited than the
536 vapor density excess version for overlaying radiosonde data. At low temperatures, the atmosphere
537 reaches saturation at small vapor density excess. Thus, the vapor density excess diagram narrows
538 drastically at low temperatures, particularly below approximately -30°C, and data points will be
539 jumbled on top of each other.

540 The package also includes functions to convert between the various moisture variables. This is
541 particularly useful for conversions to and from vapor density excess, which can be unintuitive.

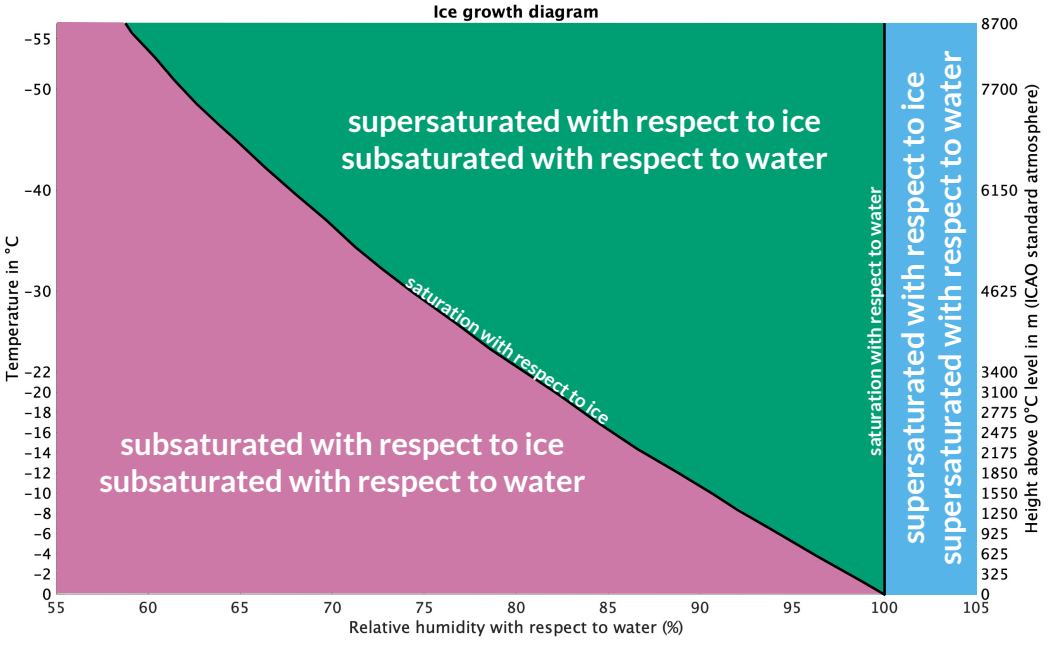

FIG. B1. Simplified diagram illustrating the phase space of subsaturated and supersaturated conditions with respect to water and ice in terms of RH_w, RH_{ice}, and air temperature. Pink shading indicates conditions where ice mass is lost by sublimation, and green shading shows conditions where ice mass grows by vapor deposition. Blue shading defines conditions where ice mass grows by vapor deposition and supercooled water droplets are constant or growing in mass. Riming can occur when supercooled water coexists with ice.

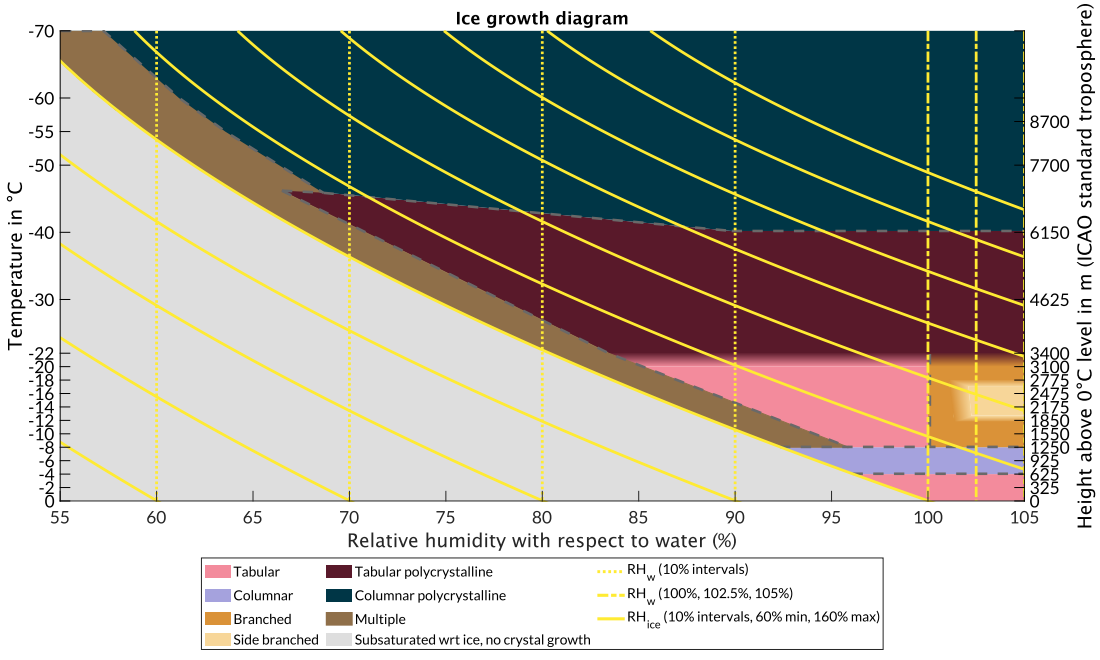

FIG. B2. The applied ice growth diagram in terms of RH_w with contours of RH_{ice} overlaid. This version is designed to have a high-contrast color scheme, appropriate for use as a base layer for data visualization.

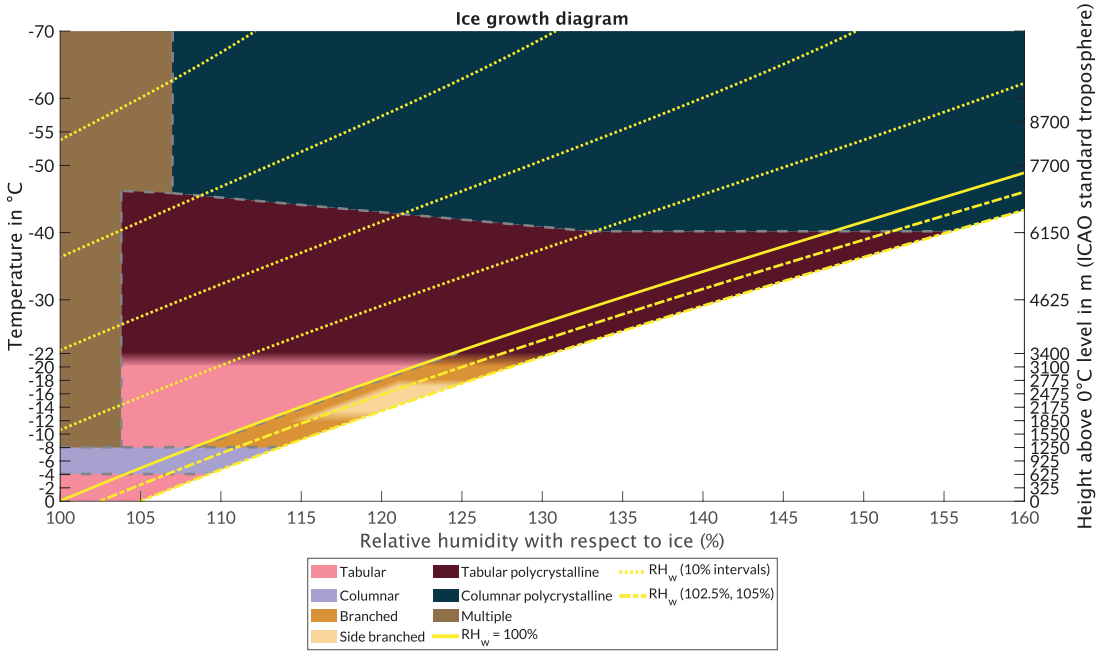

549 FIG. B3. The applied ice growth diagram in terms of RH_{ice} with contours of RH_w overlaid. This version is
550 designed to have a high-contrast color scheme, appropriate for use as a base layer for data visualization.

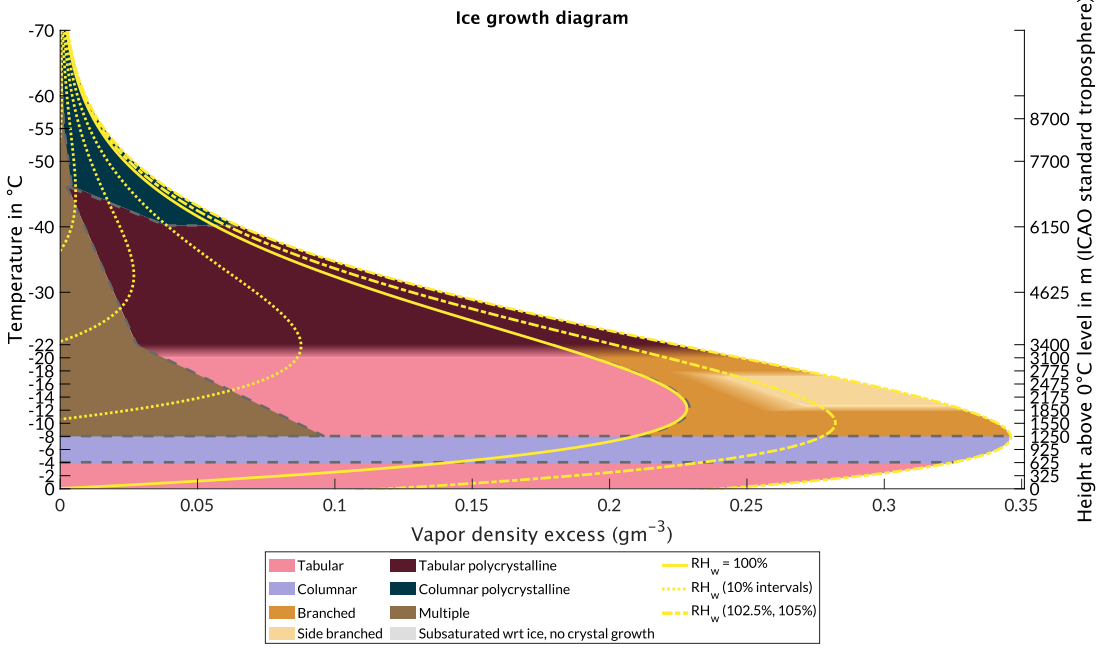

FIG. B4. The applied ice growth diagram in terms of vapor density excess with contours of RH_w overlaid. This version is designed to have a high-contrast color scheme, appropriate for use as a base layer for data visualization.

References

Abdelmonem, A., E. Järvinen, D. Duft, E. Hirst, S. Vogt, T. Leisner, and M. Schnaiter, 2016: PHIPS–HALO: the airborne Particle Habit Imaging and Polar Scattering probe – Part 1: Design and operation. *Atmospheric Measurement Techniques*, **9 (7)**, 3131–3144, https://doi.org/https://doi.org/10.5194/amt-9-3131-2016, URL https://amt.copernicus.org/articles/9/3131/2016/.

Ahrens, C. D., and R. Henson, 2018: *Meteorology Today: An Introduction to Weather, Climate and the Environment*. 12th ed., Cengage Learning, Boston, MA.

aufm Kampe, H. J., H. K. Weickmann, and J. J. Kelly, 1951: The influence of temperature on the shape of ice crystals growing at water saturation. *J. Meteor.*, **8 (3)**, 168–174, https://doi.org/10.1175/1520-0469(1951)008<0168:TIOTOT>2.0.CO;2, URL https://journals.ametsoc.org/doi/abs/10.1175/1520-0469%281951%29008%3C0168%3ATIOTOT%3E2.0.CO%3B2.

Bailey, M., and J. Hallett, 2002: Nucleation effects on the habit of vapour grown ice crystals from -18 to -42°C. *Q.J.R. Meteorol. Soc.*, **128 (583)**, 1461–1483, https://doi.org/10.1002/qj.200212858304, URL http://doi.wiley.com/10.1002/qj.200212858304.

Bailey, M., and J. Hallett, 2004: Growth Rates and Habits of Ice Crystals between -20° and -70°C. *J. Atmos. Sci.*, **61 (5)**, 514–544, https://doi.org/10.1175/1520-0469(2004)061<0514:GRAHOI>2.0.CO;2, URL http://journals.ametsoc.org/doi/full/10.1175/1520-0469%282004%29061%3C0514%3AGRAHOI%3E2.0.CO%3B2.

Bailey, M., and J. Hallett, 2010: Laboratory Measured Ice Crystal Capacitances & Mass Dimensional Relations, Portland, OR. 16.

Bailey, M., and J. Hallett, 2012: Ice Crystal Linear Growth Rates from -20° to -70°C: Confirmation from Wave Cloud Studies. *J. Atmos. Sci.*, **69 (1)**, 390–402, https://doi.org/10.1175/JAS-D-11-035.1, URL http://journals.ametsoc.org/doi/10.1175/JAS-D-11-035.1.

Bailey, M. P., and J. Hallett, 2009: A Comprehensive Habit Diagram for Atmospheric Ice Crystals: Confirmation from the Laboratory, AIRS II, and Other Field Studies. *J. Atmos. Sci.*, **66 (9)**, 2888–2899, https://doi.org/10.1175/2009JAS2883.1, URL http://journals.ametsoc.org/doi/10.1175/2009JAS2883.1.

Burton, W. K., N. Cabrera, F. C. Frank, and N. F. Mott, 1951: The growth of crystals and the equilibrium structure of their surfaces. *Philosophical Transactions of the Royal Society of London. Series A, Mathematical and Physical Sciences*, **243 (866)**, 299–358, https://doi.org/10.1098/rsta.1951.0006, URL https://royalsocietypublishing.org/doi/abs/10.1098/rsta.1951.0006, publisher: Royal Society.

Cronce, M., R. M. Rauber, K. R. Knupp, B. F. Jewett, J. T. Walters, and D. Phillips, 2007: Vertical Motions in Precipitation Bands in Three Winter Cyclones. *J. Appl. Meteor. Climatol.*, **46 (10)**, 1523–1543, https://doi.org/10.1175/JAM2533.1, URL https://journals.ametsoc.org/doi/full/10.1175/JAM2533.1.

Crowther, A. G., and C. P. R. Saunders, 1973: Ice crystal growth in electric fields. *Journal of the Meteorological Society of Japan. Ser. II*, **51 (5)**, 318–324, https://doi.org/10.2151/jmsj1965.51.5_318.

D'Alessandro, J. J., and Coauthors, 2017: Dynamical conditions of ice supersaturation and ice nucleation in convective systems: A comparative analysis between in situ aircraft observations and WRF simulations. *Journal of Geophysical Research: Atmospheres*, **122 (5)**, 2844–2866, https://doi.org/10.1002/2016JD025994, URL https://onlinelibrary.wiley.com/doi/abs/10.1002/2016JD025994.

Demange, G., H. Zapolsky, R. Patte, and M. Brunel, 2017: A phase field model for snow crystal growth in three dimensions. *npj Comput Mater*, **3 (1)**, 15, https://doi.org/10.1038/s41524-017-0015-1, URL http://www.nature.com/articles/s41524-017-0015-1.

DOE-ARM, 2020: Balloon-Borne Sounding System (SONDEWNPN). North Slope Alaska (NSA) Central Facility, Barrow AK (C1), https://doi.org/10.5439/1021460.

Durre, I., R. S. Vose, and D. B. Wuertz, 2006: Overview of the Integrated Global Radiosonde Archive. *J. Climate*, **19 (1)**, 53–68, https://doi.org/10.1175/JCLI3594.1, URL https://journals.ametsoc.org/jcli/article/19/1/53/30886/Overview-of-the-Integrated-Global-Radiosonde.

Frank, F., 1952: Crystal growth and dislocations. *Advances in Physics*, **1 (1)**, 91–109, https://doi.org/10.1080/00018735200101171, URL https:

//doi.org/10.1080/00018735200101171, publisher: Taylor & Francis _eprint: https://doi.org/10.1080/00018735200101171.

Frank, F. C., 1982: Snow crystals. *Contemporary Physics*, **23 (1)**, 3–22, https://doi.org/10.1080/00107518208231565, URL https://doi.org/10.1080/00107518208231565, publisher: Taylor & Francis _eprint: https://doi.org/10.1080/00107518208231565.

Fridlind, A. M., R. Atlas, B. van Diedenhoven, J. Um, G. M. McFarquhar, A. S. Ackerman, E. J. Moyer, and R. P. Lawson, 2016: Derivation of physical and optical properties of mid-latitude cirrus ice crystals for a size-resolved cloud microphysics model. *Atmospheric Chemistry and Physics*, **16 (11)**, 7251–7283, https://doi.org/10.5194/acp-16-7251-2016, URL https://acp.copernicus.org/articles/16/7251/2016/acp-16-7251-2016.html, publisher: Copernicus GmbH.

Fridlind, A. M., B. v. Diedenhoven, A. S. Ackerman, A. Avramov, A. Mrowiec, H. Morrison, P. Zuidema, and M. D. Shupe, 2012: A FIRE-ACE/SHEBA Case Study of Mixed-Phase Arctic Boundary Layer Clouds: Entrainment Rate Limitations on Rapid Primary Ice Nucleation Processes. *Journal of the Atmospheric Sciences*, **69 (1)**, 365–389, https://doi.org/10.1175/JAS-D-11-052.1, URL https://journals.ametsoc.org/view/journals/atsc/69/1/jas-d-11-052.1.xml, publisher: American Meteorological Society Section: Journal of the Atmospheric Sciences.

Fukuta, N., and T. Takahashi, 1999: The Growth of Atmospheric Ice Crystals: A Summary of Findings in Vertical Supercooled Cloud Tunnel Studies. *Journal of the Atmospheric Sciences*, **56 (12)**, 1963–1979, https://doi.org/10.1175/1520-0469(1999)056<1963:TGOAIC>2.0.CO;2, URL https://journals.ametsoc.org/view/journals/atsc/56/12/1520-0469_1999_056_1963_tgoaic_2.0.co_2.xml.

Furukawa, Y., and T. Kobayashi, 1978: On the growth mechanism of polycrystalline snow crystals with a specific grain boundary. *Journal of Crystal Growth*, **45**, 57–65, https://doi.org/10.1016/0022-0248(78)90415-3, URL https://linkinghub.elsevier.com/retrieve/pii/0022024878904153.

Furukawa, Y., and J. S. Wettlaufer, 2007: Snow and ice crystals. *Physics Today*, **60 (12)**, 70–71, https://doi.org/10.1063/1.2825081, URL https://physicstoday.scitation.org/doi/10.1063/1.2825081.

Gallagher, M. W., and Coauthors, 2005: An overview of the microphysical structure of cirrus clouds observed during EMERALD-1. *Quarterly Journal of the Royal Meteorological Society*, **131 (607)**, 1143–1169, https://doi.org/10.1256/qj.03.138, URL https://onlinelibrary.wiley.com/doi/abs/10.1256/qj.03.138, _eprint: https://onlinelibrary.wiley.com/doi/pdf/10.1256/qj.03.138.

Gallagher, M. W., and Coauthors, 2012: Observations and modelling of microphysical variability, aggregation and sedimentation in tropical anvil cirrus outflow regions. *Atmospheric Chemistry and Physics*, **12 (14)**, 6609–6628, https://doi.org/10.5194/acp-12-6609-2012, URL https://acp.copernicus.org/articles/12/6609/2012/, publisher: Copernicus GmbH.

Ganetis, S. A., B. A. Colle, S. E. Yuter, and N. P. Hoban, 2018: Environmental Conditions Associated with Observed Snowband Structures within Northeast U.S. Winter Storms. *Mon. Wea. Rev.*, **146 (11)**, 3675–3690, https://doi.org/10.1175/MWR-D-18-0054.1, URL https://journals.ametsoc.org/doi/abs/10.1175/MWR-D-18-0054.1.

Garrett, T. J., C. Fallgatter, K. Shkurko, and D. Howlett, 2012: Fall speed measurement and high-resolution multi-angle photography of hydrometeors in free fall. *Atmos. Meas. Tech.*, **5 (11)**, 2625–2633, https://doi.org/10.5194/amt-5-2625-2012, URL https://www.atmos-meas-tech.net/5/2625/2012/.

Gerber, H., 1991: Supersaturation and Droplet Spectral Evolution in Fog. *J. Atmos. Sci.*, **48 (24)**, 2569–2588, https://doi.org/10.1175/1520-0469(1991)048<2569:SADSEI>2.0.CO;2, URL https://journals.ametsoc.org/jas/article/48/24/2569/22870/Supersaturation-and-Droplet-Spectral-Evolution-in.

Hakim, G. J., and J. Patoux, 2017: *Weather A Concise Introduction*. Academic Press.

Hall, W. D., and H. R. Pruppacher, 1976: The Survival of Ice Particles Falling from Cirrus Clouds in Subsaturated Air. *Journal of the Atmospheric Sciences*, **33 (10)**, 1995–2006, https://doi.org/10.1175/1520-0469(1976)033<1995:TSOIPF>2.0.CO;2, URL https://journals.ametsoc.org/view/journals/atsc/33/10/1520-0469_1976_033_1995_tsoipf_2_0_co_2.xml.

Hallett, J., 1961: The growth of ice crystals on freshly cleaved covellite surfaces. *The Philosophical Magazine: A Journal of Theoretical Experimental and Applied Physics*, **6 (69)**, 1073–1087, https://doi.org/10.1080/14786436108239669, URL

https://doi.org/10.1080/14786436108239669, publisher: Taylor & Francis _eprint: https://doi.org/10.1080/14786436108239669.

Hallett, J., and B. Mason, 1958: The influence of temperature and supersaturation on the habit of ice crystals grown from the vapour. *Proc. R. Soc. Lond. A*, **247 (1251)**, 440–453, https://doi.org/10.1098/rspa.1958.0199, URL https://royalsocietypublishing.org/doi/10.1098/rspa.1958.0199.

Hallett, J., and S. C. Mossop, 1974: Production of secondary ice particles during the riming process. *Nature*, **249 (5452)**, 26–28, https://doi.org/10.1038/249026a0, URL https://www.nature.com/articles/249026a0/, number: 5452 Publisher: Nature Publishing Group.

Harrison, A., A. M. Moyle, M. Hanson, and J. Y. Harrington, 2016: Levitation Diffusion Chamber Measurements of the Mass Growth of Small Ice Crystals from Vapor. *J. Atmos. Sci.*, **73 (7)**, 2743–2758, https://doi.org/10.1175/JAS-D-15-0234.1, URL http://journals.ametsoc.org/doi/10.1175/JAS-D-15-0234.1.

Heim, F., 1914: Diamantstaub und Schneekristalle in der Antarktis (Wedellsee). *Meteorologische Zeitschrift*, **31**, 232–235.

Heymsfield, A., 1975: Cirrus Uncinus Generating Cells and the Evolution of Cirriform Clouds. Part III: Numerical Computations of the Growth of the Ice Phase. *Journal of the Atmospheric Sciences*, **32 (4)**, 820–830, https://doi.org/10.1175/1520-0469(1975)032<0820:CUGCAT>2.0.CO;2, URL https://journals.ametsoc.org/view/journals/atsc/32/4/1520-0469_1975_032_0820_cugcat_2_0_co_2.xml.

Hobbs, P. V., and W. D. Scott, 1965: A theoretical study of the variation of ice crystal habits with temperature. *Journal of Geophysical Research (1896-1977)*, **70 (20)**, 5025–5034, https://doi.org/10.1029/JZ070i020p05025, URL https://onlinelibrary.wiley.com/doi/abs/10.1029/JZ070i020p05025, _eprint: https://onlinelibrary.wiley.com/doi/pdf/10.1029/JZ070i020p05025.

Hoffmann, F., 2020: Crystal Shapes and Bravais Lattices. *Introduction to Crystallography*, F. Hoffmann, Ed., Springer International Publishing, Cham, 33–89, https://doi.org/10.1007/978-3-030-35110-6_2, URL https://doi.org/10.1007/978-3-030-35110-6_2.

Hong, Y., and G. Liu, 2015: The Characteristics of Ice Cloud Properties Derived from CloudSat and CALIPSO Measurements. *Journal of Climate*, **28 (9)**, 3880–3901,

https://doi.org/10.1175/JCLI-D-14-00666.1, URL https://journals.ametsoc.org/view/journals/clim/28/9/jcli-d-14-00666.1.xml, publisher: American Meteorological Society Section: Journal of Climate.

Houze, R. A., Jr., 2014: *Cloud dynamics*. Amsterdam ; New York : Academic Press is an imprint of Elsevier, [2014], URL catalog.lib.ncsu.edu/catalog/NCSU4492272.

ICAO, 1993: *Manual of the ICAO Standard Atmosphere: extended to 80 kilometres (262 500 feet)*, Vol. 7488. International Civil Aviation Organization.

Iwai, K., 1986: Morphological features of combination of bullet-type snow crystals observed at Syowa Station, Antarctica. *Memoirs of National Institute of Polar Research, Special Issue*, National Institute of Polar Research, Tokyo, Vol. 45, 38–46, iSBN: 0386-0744.

Järvinen, E., and Coauthors, 2018: Additional global climate cooling by clouds due to ice crystal complexity. *Atmospheric Chemistry and Physics*, **18 (21)**, 15 767–15 781, https://doi.org/10.5194/acp-18-15767-2018, URL https://acp.copernicus.org/articles/18/15767/2018/.

Ji, W., and P. K. Wang, 1999: Ventilation Coefficients for Falling Ice Crystals in the Atmosphere at Low–Intermediate Reynolds Numbers. *Journal of the Atmospheric Sciences*, **56 (6)**, 829–836, https://doi.org/10.1175/1520-0469(1999)056<0829:VCFFIC>2.0.CO;2, URL https://journals.ametsoc.org/view/journals/atsc/56/6/1520-0469_1999_056_0829_vcffic_2.0.co_2.xml.

Johnson, D. E., 1997: A study of ice microphysical and dynamical processes in a deep cyclonic front range winter storm. phdthesis, The University of Wisconsin - Madison, Ann Arbor, URL https://proxying.lib.ncsu.edu/index.php/login?url=https://www.proquest.com/dissertations-theses/study-ice-microphysical-dynamical-processes-deep/docview/304383156/se-2?accountid=12725.

Järvinen, E., and Coauthors, 2016: Quasi-Spherical Ice in Convective Clouds. *Journal of the Atmospheric Sciences*, **73 (10)**, 3885–3910, https://doi.org/10.1175/JAS-D-15-0365.1, URL https://journals.ametsoc.org/view/journals/atsc/73/10/jas-d-15-0365.1.xml, publisher: American Meteorological Society Section: Journal of the Atmospheric Sciences.

Keller, V., and J. Hallett, 1982: Influence of air velocity on the habit of ice crystal growth from the vapor. *Journal of Crystal Growth*, **60 (1)**, 91–106, https://doi.org/10.1016/0022-0248(82)90176-2, URL https://linkinghub.elsevier.com/retrieve/pii/0022024882901762.

Kikuchi, K., T. Kameda, K. Higuchi, and A. Yamashita, 2013: A global classification of snow crystals, ice crystals, and solid precipitation based on observations from middle latitudes to polar regions. *Atmospheric Research*, **132-133**, 460–472, https://doi.org/10.1016/j.atmosres.2013.06.006, URL http://www.sciencedirect.com/science/article/pii/S0169809513001841.

Kobayashi, T., 1957: Experimental Researches en the Snow Crystal Habit and Growth by Means of a Diffusion Cloud Chamber. *Journal of the Meteorological Society of Japan*, **35A (0)**, 38–47, https://doi.org/10.2151/jmsj1923.35A.0_38, URL https://www.jstage.jst.go.jp/article/jmsj1923/35A/0/35A_38/_article.

Kobayashi, T., 1961: The growth of snow crystals at low supersaturations. *Philosophical Magazine*, **6 (71)**, 1363–1370, https://doi.org/10.1080/14786436108241231, URL http://www.tandfonline.com/doi/abs/10.1080/14786436108241231.

Kobayashi, T., Y. Furukawa, K. Kikuchi, and H. Uyeda, 1976: On twinned structures in snow crystals. *Journal of Crystal Growth*, **32 (2)**, 233–249, https://doi.org/10.1016/0022-0248(76)90038-5, URL https://www.sciencedirect.com/science/article/pii/0022024876900385.

Korolev, A., and Coauthors, 2020: A new look at the environmental conditions favorable to secondary ice production. *Atmospheric Chemistry and Physics*, **20 (3)**, 1391–1429, https://doi.org/10.5194/acp-20-1391-2020, URL https://acp.copernicus.org/articles/20/1391/2020/, publisher: Copernicus GmbH.

Korolev, A. V., G. A. Isaac, and J. Hallett, 1999: Ice particle habits in Arctic clouds. *Geophysical Research Letters*, **26 (9)**, 1299–1302, https://doi.org/10.1029/1999GL900232, URL https://agupubs.onlinelibrary.wiley.com/doi/abs/10.1029/1999GL900232.

Korolev, A. V., and I. P. Mazin, 2003: Supersaturation of Water Vapor in Clouds. *Journal of the Atmospheric Sciences*, **60**, 18.

Kumjian, M. R., S. A. Rutledge, R. M. Rasmussen, P. C. Kennedy, and M. Dixon, 2014: High-Resolution Polarimetric Radar Observations of Snow-Generating Cells. *J. Appl. Me-*

teor. Climatol., **53 (6)**, 1636–1658, https://doi.org/10.1175/JAMC-D-13-0312.1, URL http://journals.ametsoc.org/doi/abs/10.1175/JAMC-D-13-0312.1.

Lauber, A., A. Kiselev, T. Pander, P. Handmann, and T. Leisner, 2018: Secondary Ice Formation during Freezing of Levitated Droplets. *Journal of the Atmospheric Sciences*, **75 (8)**, 2815–2826, https://doi.org/10.1175/JAS-D-18-0052.1, URL https://journals.ametsoc.org/view/journals/atsc/75/8/jas-d-18-0052.1.xml.

Lawson, R. P., B. Baker, B. Pilson, and Q. Mo, 2006: In Situ Observations of the Microphysical Properties of Wave, Cirrus, and Anvil Clouds. Part II: Cirrus Clouds. *J. Atmos. Sci.*, **63 (12)**, 3186–3203, https://doi.org/10.1175/JAS3803.1, URL https://journals.ametsoc.org/doi/full/10.1175/JAS3803.1.

Lawson, R. P., B. A. Baker, C. G. Schmitt, and T. L. Jensen, 2001: An overview of microphysical properties of Arctic clouds observed in May and July 1998 during FIRE ACE. *Journal of Geophysical Research: Atmospheres*, **106 (D14)**, 14 989–15 014, https://doi.org/10.1029/2000JD900789, URL https://agupubs.onlinelibrary.wiley.com/doi/abs/10.1029/2000JD900789.

Lawson, R. P., and Coauthors, 2019: A Review of Ice Particle Shapes in Cirrus formed In Situ and in Anvils. *Journal of Geophysical Research: Atmospheres*, **124 (17-18)**, 10 049–10 090, https://doi.org/10.1029/2018JD030122, URL http://agupubs.onlinelibrary.wiley.com/doi/abs/10.1029/2018JD030122.

Libbrecht, K. G., 2003: Explaining the formation of thin ice crystal plates with structure-dependent attachment kinetics. *Journal of Crystal Growth*, **258 (1)**, 168–175, https://doi.org/10.1016/S0022-0248(03)01496-9, URL http://www.sciencedirect.com/science/article/pii/S0022024803014969.

Libbrecht, K. G., 2005: The physics of snow crystals. *Rep. Prog. Phys.*, **68 (4)**, 855–895, https://doi.org/10.1088/0034-4885/68/4/R03, URL http://stacks.iop.org/0034-4885/68/i=4/a=R03?key=crossref.20ee6058f7eef929c9682b9083b19de8.

Libbrecht, K. G., 2017: Physical Dynamics of Ice Crystal Growth. *Annu. Rev. Mater. Res.*, **47 (1)**, 271–295, https://doi.org/10.1146/annurev-matsci-070616-124135, URL https://doi.org/10.1146/annurev-matsci-070616-124135.

Libbrecht, K. G., 2020: Guide to Snowflakes - SnowCrystals.com. URL http://www.snowcrystals.com/morphology/morphology.html.

Liou, K.-N., 1986: Influence of Cirrus Clouds on Weather and Climate Processes: A Global Perspective. *Monthly Weather Review*, **114 (6)**, 1167–1199, https://doi.org/10.1175/1520-0493(1986)114<1167:IOCCOW>2.0.CO;2, URL https://journals.ametsoc.org/view/journals/mwre/114/6/1520-0493_1986_114_1167_ioccow_2_0_co_2.xml, publisher: American Meteorological Society Section: Monthly Weather Review.

Liou, K.-N., and P. Yang, 2016: *Light Scattering by Ice Crystals: Fundamentals and Applications*. Cambridge University Press, google-Books-ID: 7PoODQAAQBAJ.

Magee, N., and Coauthors, 2021: Captured cirrus ice particles in high definition. *Atmospheric Chemistry and Physics*, **21 (9)**, 7171–7185, https://doi.org/10.5194/acp-21-7171-2021, URL https://acp.copernicus.org/articles/21/7171/2021/, publisher: Copernicus GmbH.

Magono, C., and C. W. Lee, 1966: Meteorological Classification of Natural Snow Crystals. *Journal of the Faculty of Science:Hokkaido University*, **4 (2)**, 45.

Mason, B. J., 1953: The growth of ice crystals in a supercooled water cloud. *Quarterly Journal of the Royal Meteorological Society*, **79 (339)**, 104–111, https://doi.org/10.1002/qj.49707933909, URL https://rmets.onlinelibrary.wiley.com/doi/abs/10.1002/qj.49707933909.

Mason, B. J., G. W. Bryant, and A. P. Van den Heuvel, 1963: The growth habits and surface structure of ice crystals. *The Philosophical Magazine: A Journal of Theoretical Experimental and Applied Physics*, **8 (87)**, 505–526, https://doi.org/10.1080/14786436308211150, URL https://doi.org/10.1080/14786436308211150, publisher: Taylor & Francis _eprint: https://doi.org/10.1080/14786436308211150.

Mason, B. J. B. J., 1971: *The physics of clouds*. 2nd ed., Oxford monographs on meteorology., Clarendon Press, Oxford.

McMurdie, L. A., G. M. Heymsfield, S. A. Braun, and J. E. Yorks, 2019: IMPACTS: A NASA Earth-Venture Suborbital-3 Airborne Field Campaign to Investigate U.S. East Coast Snowstorms. AMS, URL https://ams.confex.com/ams/18MESO/meetingapp.cgi/Paper/361168.

McMurdie, L. A., and Coauthors, 2022: Chasing Snowstorms: The Investigation of Microphysics and Precipitation for Atlantic Coast-threatening Snowstorms. *Bulletin of the American Meteorological Society*, conditionally accepted.

Midzak, N., J. E. Yorks, J. Zhang, B. v. Diedenhoven, S. Woods, and M. McGill, 2020: A Classification of Ice Crystal Habits Using Combined Lidar and Scanning Polarimeter Observations during the SEAC4RS Campaign. *Journal of Atmospheric and Oceanic Technology*, **37 (12)**, 2185–2196, https://doi.org/10.1175/JTECH-D-20-0037.1, URL https://journals.ametsoc.org/view/journals/atot/37/12/jtech-d-20-0037.1.xml, publisher: American Meteorological Society Section: Journal of Atmospheric and Oceanic Technology.

Miller, M., and Coauthors, 2017: Complex aggregates within coastal northeast U.S. snow storms. 17th Conference on Mesoscale Processes, URL https://ams.confex.com/ams/17MESO/webprogram/Paper320116.html.

Nakaya, U., and Y. Sekido, 1936: General classification of snow crystals and their frequency of occurrence. *Journal of the Faculty of Science, Hokkaido Imperial University. Ser. 2, Physics*, **1 (9)**, 243–264.

Nakaya, U., 1900-1962, 1954: *Snow crystals, natural and artificial.* Cambridge : Harvard University Press, 1954., URL catalog.lib.ncsu.edu/catalog/NCSU164744.

NASA, 2020: IMPACTS. URL https://espo.nasa.gov/impacts/content/IMPACTS.

Nelson, J., 2005: Branch Growth and Sidebranching in Snow Crystals. *Crystal Growth & Design*, **5 (4)**, 1509–1525, https://doi.org/10.1021/cg049685v, URL https://doi.org/10.1021/cg049685v, publisher: American Chemical Society.

Nelson, J., and C. Knight, 1998: Snow Crystal Habit Changes Explained by Layer Nucleation. *Journal of the Atmospheric Sciences*, **55 (8)**, 1452–1465, https://doi.org/10.1175/1520-0469(1998)055<1452:SCHCEB>2.0.CO;2, URL https://journals.ametsoc.org/view/journals/atsc/55/8/1520-0469_1998_055_1452_schceb_2.0.co_2.xml, publisher: American Meteorological Society Section: Journal of the Atmospheric Sciences.

Nelson, J., and B. D. Swanson, 2019: Lateral facet growth of ice and snow – Part 1: Observations and applications to secondary habits. *Atmospheric Chemistry and Physics*, **19 (24)**, 15 285–

15 320, https://doi.org/10.5194/acp-19-15285-2019, URL https://acp.copernicus.org/articles/19/15285/2019/, publisher: Copernicus GmbH.

NWS, A., 2017: Winter Precipitation Types. URL https://www.weather.gov/ama/winterpreciptypes, publication Title: National Weather Service Amarillo, TX.

Otte, H. M., and A. G. Crocker, 1965: Crystallographic Formulae for Hexagonal Lattices. *physica status solidi (b)*, **9 (2)**, 441–450, https://doi.org/10.1002/pssb.19650090217, URL https://onlinelibrary.wiley.com/doi/abs/10.1002/pssb.19650090217.

Pruppacher, H. R., 1930, and J. D. Klett, 1940, 1997: *Microphysics of clouds and precipitation*. Dordrecht ; Boston : Kluwer Academic Publishers, [1997], URL catalog.lib.ncsu.edu/catalog/NCSU949108.

Rauber, R. M., S. M. Ellis, J. Vivekanandan, J. Stith, W.-C. Lee, G. M. McFarquhar, B. F. Jewett, and A. Janiszeski, 2017: Finescale Structure of a Snowstorm over the Northeastern United States: A First Look at High-Resolution HIAPER Cloud Radar Observations. *Bull. Amer. Meteor. Soc.*, **98 (2)**, 253–269, https://doi.org/10.1175/BAMS-D-15-00180.1, URL https://journals.ametsoc.org/doi/full/10.1175/BAMS-D-15-00180.1.

Rauber, R. M., and S. W. Nesbitt, 2018: *Radar meteorology : a first course*. Hoboken, NJ : John Wiley & Sons, 2018., Hoboken, NJ, URL catalog.lib.ncsu.edu/catalog/NCSU4750020.

Rogers, R. R., and M. K. Yau, 1989: *A Short Course in Cloud Physics*, International Series in Natural Philosophy, Vol. 113. 3rd ed., Pergamon Press.

Ryan, B. F., E. R. Wishart, and D. E. Shaw, 1976: The Growth Rates and Densities of Ice Crystals between -3°C and -21°C. *Journal of the Atmospheric Sciences*, **33 (5)**, 842–850, https://doi.org/10.1175/1520-0469(1976)033<0842:TGRADO>2.0.CO;2, URL https://journals.ametsoc.org/view/journals/atsc/33/5/1520-0469_1976_033_0842_tgrado_2_0_co_2.xml, publisher: American Meteorological Society Section: Journal of the Atmospheric Sciences.

Sassen, K., Z. Wang, and D. Liu, 2008: Global distribution of cirrus clouds from CloudSat/Cloud-Aerosol Lidar and Infrared Pathfinder Satellite Observations (CALIPSO) measurements. *Journal of Geophysical Research: Atmospheres*, **113 (D8)**, https://doi.org/

855 10.1029/2008JD009972, URL https://onlinelibrary.wiley.com/doi/abs/10.1029/2008JD009972,
856 _eprint: https://onlinelibrary.wiley.com/doi/pdf/10.1029/2008JD009972.

857 Sazaki, G., S. Zepeda, S. Nakatsubo, E. Yokoyama, and Y. Furukawa, 2010: Elementary steps at
858 the surface of ice crystals visualized by advanced optical microscopy. *Proceedings of the Na-*
859 *tional Academy of Sciences*, **107 (46)**, 19 702–19 707, https://doi.org/10.1073/pnas.1008866107,
860 URL https://www.pnas.org/doi/abs/10.1073/pnas.1008866107, publisher: Proceedings of the
861 National Academy of Sciences.

862 Schnaiter, F. M., 2020: Particle Habit Imaging and Polar Scattering Probe (PHIPS) IMPACTS.
863 NASA Global Hydrology Resource Center DAAC, Huntsville, Alabama, U.S.A, URL http:
864 //dx.doi.org/10.5067/IMPACTS/PHIPS/DATA101.

865 St-Pierre, M., and J. M. Thériault, 2015: Clarification of the Water Saturation Repre-
866 sented on Ice Crystal Growth Diagrams. *J. Atmos. Sci.*, **72 (7)**, 2608–2611, https://doi.org/
867 10.1175/JAS-D-14-0357.1, URL http://journals.ametsoc.org/doi/10.1175/JAS-D-14-0357.1.

868 Takahashi, T., 2014: Influence of Liquid Water Content and Temperature on the Form and Growth
869 of Branched Planar Snow Crystals in a Cloud. *Journal of the Atmospheric Sciences*, **71 (11)**,
870 4127–4142, https://doi.org/10.1175/JAS-D-14-0043.1, URL https://journals.ametsoc.org/view/
871 journals/atsc/71/11/jas-d-14-0043.1.xml, publisher: American Meteorological Society Section:
872 Journal of the Atmospheric Sciences.

873 Takahashi, T., T. Endoh, G. Wakahama, and N. Fukuta, 1991: Vapor Diffusional Growth of Free-
874 Falling Snow Crystals between -3 and -23 deg C. *Journal of the Meteorological Society of Japan.*
875 *Ser. II*, **69 (1)**, 15–30, https://doi.org/10.2151/jmsj1965.69.1_15, URL https://www.jstage.jst.go.
876 jp/article/jmsj1965/69/1/69_1_15/_article/-char/en.

877 UCAR, 2020: *Snowpack and its Assessment: Snow Microphysics*. 2009th ed., Comet Meted, The
878 University Corporation for Atmospheric Research, Boulder, CO, URL https://www.meted.ucar.
879 edu/training_module.php?id=431&tab=01.

880 Vázquez-Martín, S., T. Kuhn, and S. Eliasson, 2020: Shape Dependence of Falling Snow Crystals'
881 Microphysical Properties Using an Updated Shape Classification. *Applied Sciences*, **10 (3)**, 1163.

882 Wang, P. K., 2002: *Ice microdynamics*. Academic Press, San Diego, Calif.

Wang, P. K., 2013: *Physics and dynamics of clouds and precipitation*. Cambridge : Cambridge University Press, 2013., URL catalog.lib.ncsu.edu/catalog/NCSU4689464.

Weickmann, H., 1945: Formen und bildung atmosphaerischer eiskristalle. *Beiträge zur Physik der Atmosphäre*, **28**, 12–52.

Wendisch, M., and P. Yang, 2012: *Theory of atmospheric radiative transfer: a comprehensive introduction*. John Wiley & Sons.

Wood, S. E., M. B. Baker, and D. Calhoun, 2001: New model for the vapor growth of hexagonal ice crystals in the atmosphere. *Journal of Geophysical Research: Atmospheres*, **106 (D5)**, 4845–4870, https://doi.org/10.1029/2000JD900338, URL https://onlinelibrary.wiley.com/doi/abs/10.1029/2000JD900338, _eprint: https://onlinelibrary.wiley.com/doi/pdf/10.1029/2000JD900338.

Woods, S., R. P. Lawson, E. Jensen, T. P. Bui, T. Thornberry, A. Rollins, L. Pfister, and M. Avery, 2018: Microphysical Properties of Tropical Tropopause Layer Cirrus. *Journal of Geophysical Research: Atmospheres*, **123 (11)**, 6053–6069, https://doi.org/10.1029/2017JD028068, URL https://onlinelibrary.wiley.com/doi/abs/10.1029/2017JD028068, _eprint: https://onlinelibrary.wiley.com/doi/pdf/10.1029/2017JD028068.

Yang, P., S. Hioki, M. Saito, C.-P. Kuo, B. A. Baum, and K.-N. Liou, 2018: A Review of Ice Cloud Optical Property Models for Passive Satellite Remote Sensing. *Atmosphere*, **9 (12)**, 499, https://doi.org/10.3390/atmos9120499, URL https://www.mdpi.com/2073-4433/9/12/499, number: 12 Publisher: Multidisciplinary Digital Publishing Institute.

Yang, P., and Coauthors, 2008: Effect of Cavities on the Optical Properties of Bullet Rosettes: Implications for Active and Passive Remote Sensing of Ice Cloud Properties. *Journal of Applied Meteorology and Climatology*, **47 (9)**, 2311–2330, https://doi.org/10.1175/2008JAMC1905.1, URL https://journals.ametsoc.org/view/journals/apme/47/9/2008jamc1905.1.xml.

Yang Martin, M. a. R. B., 2020: P-3 Meteorological and Navigation Data IMPACTS. NASA Global Hydrology Resource Center DAAC, Huntsville, Alabama, U.S.A, URL http://dx.doi.org/10.5067/IMPACTS/P3/DATA101.

Zhu, S., X. Guo, G. Lu, and L. Guo, 2015: Ice Crystal Habits and Growth Processes in Stratiform Clouds with Embedded Convection Examined through Aircraft Observation in North-

ern China. *Journal of the Atmospheric Sciences*, **72 (5)**, 2011–2032, https://doi.org/10.1175/JAS-D-14-0194.1, URL https://journals.ametsoc.org/view/journals/atsc/72/5/jas-d-14-0194.1.xml, publisher: American Meteorological Society Section: Journal of the Atmospheric Sciences.